Paper # 07F-70 **Topic: Detonation Linear Stability**

2007 Fall Meeting of the Western States Section of the Combustion Institute
Sandia National Laboratories, Livermore, CA
October 16 & 17, 2007.

Linear stability of detonations with reversible chemical reactions

S. T. Browne and J. E. Shepherd

California Institute of Technology, Pasadena, CA 91105 USA

The scope of our present study is the linear stage of the detonation instability of an initially steady, one-dimensional base flow based on the ZND detonation model. Our goal is to develop numerical tools that will enable the computation of stability characteristics for multi-step reaction mechanisms with reversible reactions and mixture thermodynamics with variable specific heat. To this end, we have generalized the formulation of the linear stability equations following the method of Lee and Stewart and Short. We have implemented the solution in the physical space domain as a shooting problem using Cantera to analytically evaluate all thermodynamic quantities and derivatives. The computational domain is in the flat-shock-fixed frame such that the left boundary satisfies the perturbed shock jump conditions and the right boundary satisfies a radiation condition. In the case of a reversible mechanism, the radiation condition cannot be solved analytically and a numerical method is proposed. To investigate reversibility, we have constructed a family single-step mechanisms with a fixed CJ temperature but varying extents of reversibility. We have computed the unstable modes as a function of the extent of reversibility and degree of overdrive.

1 Introduction

Experiments and numerical simulations of detonation propagation problems are characterized by unsteady motion due to the intrinsic instability of the reaction zone structure. Investigations of the detonation linear stability problem have almost exclusively been concerned with model systems using the perfect gas equation of state and reaction mechanisms consisting of a small number (usually one) of irreversible reactions [1]. Starting from the one-step model used in the pioneering studies of Erpenbeck and the reformulation of the numerical approach by Stewart and coworkers [2–4], researchers have been making steady progress by considering more complex chemical reaction models and equations of state [5, 6].

The scope of our present study is the linear stage of the instability of an initially steady, one-dimensional base flow based on the ZND model of detonation structure. Our goal is to develop numerical tools that will enable the computation of stability characteristics for multi-step reaction mechanisms with reversible reactions, realistic rate constant representation, and mixture thermodynamics with variable specific heat. To this end, we have generalized the formulation of the linear stability equations following the method of Lee and Stewart [2] and Short [3, 4].

We have verified that our method discussed in Section 2 will reproduce the previous one- and two-dimensional results of Lee and Stewart and Short and Stewart and have proceeded to examine the effect of reversibility on the one-step reaction. We have constructed a family of CJ solutions with a fixed CJ temperature but varying extents of reversibility in the reaction rate. The extent of reversibility is controlled by the entropy of the product state relative to the reactant. Using this family of CJ solutions, we have computed the unstable modes as a function of the extent of reversibility and degree of overdrive. Our results are presented in Section 3.

2 Formulation and Implementation

The system of interest is governed by the reactive Euler equations.

$$\frac{\mathrm{D}v}{\mathrm{D}t} = v\nabla\cdot\mathbf{u} \tag{1}$$

$$\frac{\mathrm{D}\mathbf{u}}{\mathrm{D}t} = -v\nabla P \tag{2}$$

$$\frac{\mathrm{D}P}{\mathrm{D}t} + \frac{a_f^2}{v}\nabla\cdot\mathbf{u} = -\frac{G}{v}\sum_{k=1}^{N}\left.\frac{\partial e}{\partial Y_k}\right|_{P,v,Y_{j\neq k}}\dot{\Omega}_k \tag{3}$$

$$\frac{\mathrm{D}Y_i}{\mathrm{D}t} = \dot{\Omega}_i \qquad i = 1,\ldots,N \tag{4}$$

$$\frac{\mathrm{D}}{\mathrm{D}t} = \frac{\partial}{\partial t} + \mathbf{u}\cdot\nabla \tag{5}$$

where v is the specific volume, (u,v) are the normal and tangential velocities, P is the pressure, $\mathbf{Y}$ is the species vector, $\dot{\Omega}_i$ is the net production rate of species i, ρ is the density, a_f is the frozen soundspeed, and G is the Grüneisen coefficient. In addition to these equations, we use the ideal gas equation of state.

2.1 Reference Frame

The reactive Euler equations given by Equations 1-4 are given in the laboratory reference frame. To solve our problem, we transform these equations to the flat-shock-fixed frame with a change of variables which places the shock at the origin of the coordinate system. The difference between this reference frame and the laboratory frame is illustrated in Figure 1. Erpenbeck first proposed this coordinate transformation [7] and emphasized the importance of linearizing the system about "the state of the unperturbed system at the same distance from the shock in order to avoid non-infinitesimal fluctuations" in thermodynamic quantities due to "infinitesimal fluctuations in the position of the shock." In the following discussion, the laboratory coordinates will be designated by a superscript L.

The location of the shock in the laboratory frame is

$$x^L_{shock} = \int^{t^L} \mathrm{D}dt = \mathrm{U}t^L + \psi(y^L, t^L). \tag{6}$$

We are interested in measuring distance relative to x^L_{shock}, so our new coordinate, x, is

$$x = x^L_{shock} - x^L = \left[\mathrm{U}t^L + \psi(y^L, t^L)\right] - x^L. \tag{7}$$

The independent variables, vertical distance (y) and time (t), remain unchanged. Thermodynamic variables are also invariant with respect to coordinate system transformations. On the other hand, the unperturbed velocity components must be transformed to the flat shock fixed frame. This only applies to the velocity component normal to the shock (u) because the mean shock velocity in the direction tangential to the shock is zero.

$$\mathrm{u} = \mathrm{U} - \mathrm{u}^L \tag{8}$$

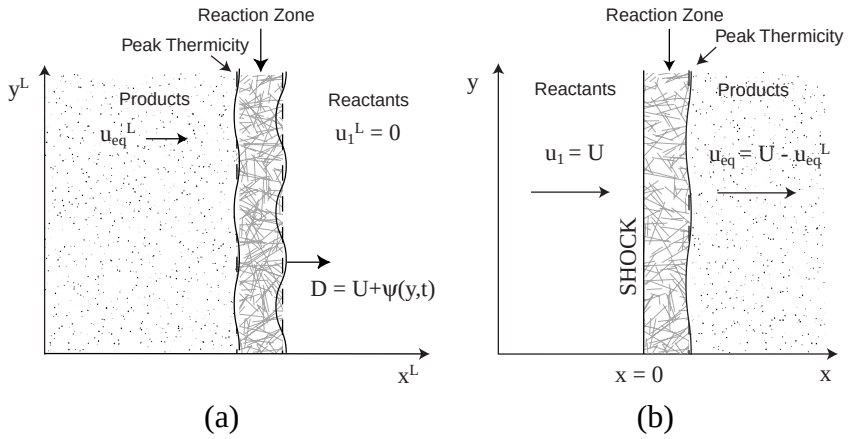

Figure 1: Two frames of reference: (a) laboratory frame and (b) flat-shock-fixed frame.

It is important to note that the transformation of u does not contain ψ because we are interested in solving for fluctuations in u. If we had accounted for ψ in the transformation of u as we have in the transformation of x, u would not have fluctuations.

Following the normal modes approach outlined in Lee and Stewart [2] and Short [3], we linearly perturb Equations 1-4. We assume that the base flow ($\mathbf{z}^o$) satisfies the steady ZND model [8–10] and that the perturbations ($\mathbf{z}^1(x,y,t)$) are proportional to ψ. The generalized dimensional governing equations in the flat-shock-fixed frame are the ZND equations

$$\mathbf{A}^o \mathbf{z}^o_{,x}(x) = \mathbf{c}^o \tag{9}$$

and the perturbation equation

$$(\mathbf{z}^1_{,t} + \mathbf{b}^o \psi_{,t}) + \mathbf{A}^o \mathbf{z}^1_{,x} + \mathbf{B}^o (\mathbf{z}^1_{,y} + \mathbf{b}^o \psi_{,y}) + \mathbf{C}^o \mathbf{z}^1 = 0 \tag{10}$$

where

$$Z(v,P,\mathbf{Y}) = -\frac{G}{v}\sum_{i=1}^{N} e_{,Y_i}\dot{\Omega}_i \tag{11}$$

$$\mathbf{b} = \mathbf{z}_{,x} \qquad \mathbf{c} = [0 \quad 0 \quad Z(v,P,\mathbf{Y}) \quad \dot{\Omega}_1 \quad \dot{\Omega}_2 \quad \dots]^T \tag{12}$$

$$\mathbf{A} = \begin{pmatrix} \mathrm{u} & -v & 0 & 0 & 0 & 0 & \dots \\ 0 & \mathrm{u} & 0 & v & 0 & 0 & \dots \\ 0 & 0 & \mathrm{u} & 0 & 0 & 0 & \dots \\ 0 & \rho a_f^2 & 0 & \mathrm{u} & 0 & 0 & \dots \\ 0 & 0 & 0 & 0 & \mathrm{u} & 0 & \dots \\ 0 & 0 & 0 & 0 & 0 & \mathrm{u} & \dots \\ \dots & & & & & & \end{pmatrix} \qquad \mathbf{B} = \begin{pmatrix} \mathrm{v} & 0 & -v & 0 & 0 & 0 & \dots \\ 0 & \mathrm{v} & 0 & 0 & 0 & 0 & \dots \\ 0 & 0 & \mathrm{v} & v & 0 & 0 & \dots \\ 0 & 0 & \rho a_f^2 & \mathrm{v} & 0 & 0 & \dots \\ 0 & 0 & 0 & 0 & \mathrm{v} & 0 & \dots \\ 0 & 0 & 0 & 0 & 0 & \mathrm{v} & \dots \\ \dots & & & & & & \end{pmatrix} \tag{13}$$

$$\mathbf{C} = \begin{pmatrix} -\mathrm{u}_{,x} & v_{,x} & 0 & 0 & 0 & 0 & \dots \\ P_{,x} & \mathrm{u}_{,x} & 0 & 0 & 0 & 0 & \dots \\ 0 & \mathrm{v}_{,x} & 0 & 0 & 0 & 0 & \dots \\ (\rho a_f^2)_{,v}\mathrm{u}_{,x} - Z_{,v} & P_{,x} & 0 & (\rho a_f^2)_{,P}\mathrm{u}_{,x} - Z_{,P} & (\rho a_f^2)_{,Y_1}\mathrm{u}_{,x} - Z_{,Y_1} & (\rho a_f^2)_{,Y_2}\mathrm{u}_{,x} - Z_{,Y_2} & \dots \\ -\dot{\Omega}_{1,v} & Y_{1,x} & 0 & -\dot{\Omega}_{1,P} & -\dot{\Omega}_{1,Y_1} & -\dot{\Omega}_{1,Y_2} & \dots \\ -\dot{\Omega}_{2,v} & Y_{2,x} & 0 & -\dot{\Omega}_{2,P} & -\dot{\Omega}_{2,Y_1} & -\dot{\Omega}_{2,Y_2} & \dots \\ \dots & & & & & & \end{pmatrix} \tag{14}$$

We assume ψ has the following functional form

$$\psi = \psi^1 \exp\left[\omega t + i k_y y\right] \tag{15}$$

and the independent variables vector ($\mathbf{z}$) becomes

$$\mathbf{z} = [v, \mathrm{u}, \mathrm{v}, P, Y_1, Y_2, \dots, Y_N]^T \tag{16}$$

$$= \mathbf{z}^o + \mathbf{z}^1(x)\psi^1 \exp\left[\omega t + i k_y y\right] \tag{17}$$

where ψ^1 is the constant magnitude of the initial perturbation, ω is the complex eigenvalue ($\mathcal{R}e(\omega) + i\,\mathcal{I}m(\omega)$), and k_y is the transverse wave number. Now, Equation 10 becomes

$$\mathbf{A}^o\mathbf{z}^1_{,x}(x) + \left[\omega\mathbf{I} + \mathbf{C}^o + i k_y \mathbf{B}^o\right]\mathbf{z}^1(x) + (\omega\mathbf{I} + i k_y \mathbf{B}^o)\mathbf{b}^o\psi^1 = 0 \tag{18}$$

The superscripts designate the base state (^{o}) and the perturbed state (^{1}). We have implemented the solution in the physical space domain as a shooting problem that requires the solution of the set of coupled ordinary differential equations for the base flow and perturbed quantities. We have used the CVODE [11] stiff solver to integrate through our domain which is ten induction lengths (Δ_{ZND}) long.

2.2 Thermodynamics and Kinetics Mechanism

Our implementation uses Cantera [12] to evaluate all thermodynamic quantities and derivatives of quantities dependent on the kinetics model. By using Cantera, the user is free to select the mechanism, thermodynamic, and reaction rate models specific to his problem. This includes the ability to use the sizable hydrocarbon fuel reaction mechanisms that have been developed by the combustion community in the last two decades as well as reduced or notional mechanisms with pseudo-species.

In previous studies, the one step irreversible model [2]

$$\mathcal{A} \overset{k_f}{\rightarrow} \mathcal{B} \tag{R1}$$

$$k_f = A \exp\left(-\frac{E_a}{\mathcal{R}T}\right) \tag{19}$$

has been extensively examined as a function of the parameters: activation energy (E_a), exothermic heat release (Q), specific heat ratio (γ), and overdrive ($f = (U/U_{CJ})^2$). The net production rates for the irreversible mechanism are

$$\dot{\Omega}_{\mathcal{A}} = -k_f Y_{\mathcal{A}} \qquad \dot{\Omega}_{\mathcal{B}} = k_f Y_{\mathcal{A}} \tag{20}$$

Most researchers have validated their implementations using Erpenbeck's case: $E/\mathcal{R}T_o = 50$, $Q/\mathcal{R}T_o = 50$, $\gamma = 1.2$, and $f = 1.2$. Using Cantera, we are able to create an input file that mimics this case. In addition, we have the flexibility to specify a reversible reaction and vary the extent of reversibility, i.e. the amount of product achieved at equilibrium, by adjusting the entropy difference between the reactant and product species.

We have chosen to create a family of systems with equal Chapman-Jouguet temperatures (T_{CJ}). Each system has one global reversible reaction

$$\mathcal{A} \overset{k_f, k_b}{\leftrightarrow} \mathcal{B} \tag{R2}$$

$$k_f = A \exp\left(-\frac{E_a}{\mathcal{R}T}\right) \tag{21}$$

$$k_b = \frac{k_f}{K_C} = k_f \exp\left[\frac{\Delta h - T\Delta s}{RT}\right] \tag{22}$$

$$= \left[A \exp\left(\frac{\Delta s}{R}\right)\right] \exp\left[-\frac{(E_a - \Delta h)}{RT}\right] \tag{23}$$

where $\mathcal{A}$ and $\mathcal{B}$ are perfect gases with equal molecular weights and ratios of specific heat ($\gamma = 1.2$). The other symbols in this system are: k_f forward reaction rate which has an Arrhenius form, k_b reverse reaction rate governed by the principle of detailed balance, K_C equilibrium constant, $\Delta h = h_{\mathcal{B}} - h_{\mathcal{A}}$ difference in specific enthalpy, and $\Delta s = s_{\mathcal{B}} - s_{\mathcal{A}}$ difference in specific entropy. In this case, the net production rates are

$$\dot{\Omega}_{\mathcal{A}} = -k_f Y_{\mathcal{A}} + k_b Y_{\mathcal{B}} \qquad \dot{\Omega}_{\mathcal{B}} = k_f Y_{\mathcal{A}} - k_b Y_{\mathcal{B}} \tag{24}$$

To vary the extent of reversibility, we specify the desired entropy difference ($\Delta s/R$) and desired T_{CJ} and iteratively solve for the required heat release ($\Delta h/RT_o$). Table 1 and Figure 2 describe the family of systems that we have created. We see that the $\Delta s/R = 0$ case is comparable to the irreversible case in that the ratio of reactant to product at equilibrium approaches zero. As $\Delta s/R$ decreases, the extent of reversibility increases and the ratio of reactant to product increases. If we choose a large negative value for $\Delta s/R$, we could construct a system that does not react.

We also require that the time scale of each system be the half-reaction time ($t_{\lambda=1/2}$). While this can be achieved several ways, we choose to vary the pre-exponential (A) in our Arrhenius rate (see Equation 21) for each degree of overdrive and extent of reversibility.

$\Delta s/R$	$\Delta h/(RT_o)$	U_{CJ}	λ_{eq}
0	50.71	1701.25	0.985
-2	53.93	1699.00	0.921
-4	63.35	1696.42	0.775
-6	78.38	1695.20	0.621
-8	96.50	1694.72	0.502

Table 1: Reversibility parameters for $T_{CJ} = 3599.29$ K

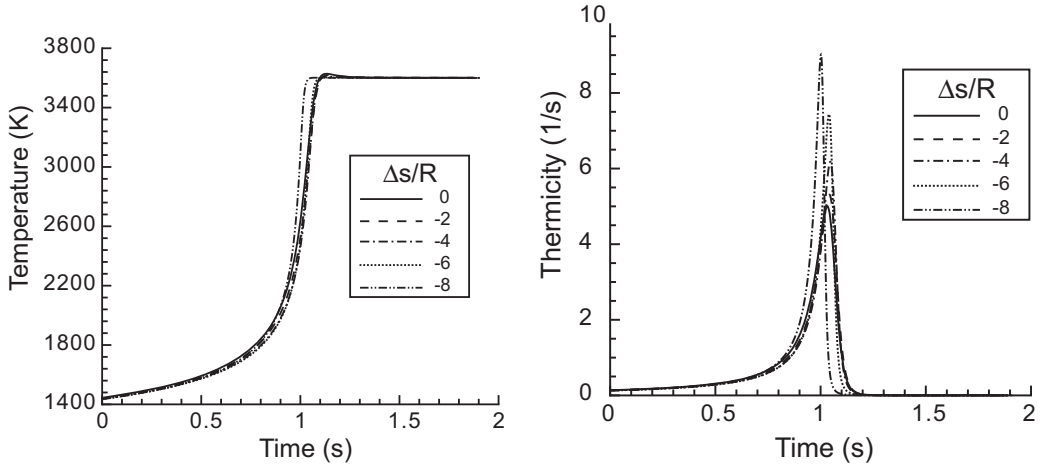

(a) (b)

Figure 2: Family of constant T_{CJ} solutions ($T_{CJ} = 3599.29\ K$). (a) Temperature profiles (b) Thermicity profiles

2.3 Boundary Conditions

The computational domain is the reaction zone in the shock-fixed frame such that the left boundary conditions are the perturbed shock jump conditions in the flat-shock-fixed reference frame. We have derived these for a general equation of state

$$v^1_{x=0} = -\omega\psi^1 v^o_{x=0}\left[\frac{v_{x=0}}{v_1}\left(\frac{\frac{v_1}{v_{x=0}}G\mathrm{U} - 2\mathrm{U}[G+1] + \mathrm{w}_{x=0}[G+2]}{(a_f^2)_{x=0}(M^2_{x=0}-1)}\right)\right]^o \tag{25}$$

$$P^1_{x=0} = \omega\psi^1\frac{\mathrm{w}^o_{x=0}}{v^o_1}\left[2\left(\frac{\mathrm{U}}{\mathrm{w}_{x=0}}-1\right) + \mathrm{w}_{x=0}\left(\frac{\frac{v_1}{v_{x=0}}G\mathrm{U} - 2\mathrm{U}[G+1] + \mathrm{w}_{x=0}[G+2]}{(a_f)^2_{x=0}(M^2_{x=0}-1)}\right)\right]^o \tag{26}$$

$$\mathrm{u}^1_{x=0} = -\omega\psi^1\left[1 - \frac{v_{x=0}}{v_1}\left(1 - \mathrm{w}_{x=0}\left(\frac{\frac{v_1}{v_{x=0}}G\mathrm{U} - 2\mathrm{U}[G+1] + \mathrm{w}_{x=0}[G+2]}{(a_f)^2_{x=0}(M^2_{x=0}-1)}\right)\right)\right]^o \tag{27}$$

$$\mathrm{v}^1_{x=0} = -(\mathrm{U} - \mathrm{w}^o_{x=0})ik_y\psi^1 \tag{28}$$

and implemented them for an ideal gas equation of state.

At the right boundary, the system must satisfy a radiation condition requiring that all waves travel out of the domain. To eliminate the incoming component of the solution, we must first decompose the solution vector into waves. We perform this decomposition far from the reaction zone where although the perturbations are non-zero, the bulk flow is no longer changing. In this regime Equation 18 simplifies to

$$\mathbf{A}^o_\infty \mathbf{z}^1_{,x}(x) + [\omega \mathbf{I} + \mathbf{C}^o_\infty + ik_y \mathbf{B}^o_\infty]\, \mathbf{z}^1(x) = 0 \tag{29}$$

In the case of a single irreversible reaction (Reaction R1), an analytic solution for the wave decomposition is presented in Lee and Stewart [2]. This analytic solution arises from the fact that far from the reaction zone, all derivatives with respect to specific volume and pressure as well as all spatial derivatives are zero. The reactant and product species mass fractions are not independent because

$$\sum_i Y_i = 1 \ . \tag{30}$$

so that Equation 10 can be expressed as a function of a single progress variable, $Y_\mathcal{B}$. Now, $\mathbf{C}$ (Equation 14) has only 2 non-zero elements, and there exists a one-way coupling between the chemistry and fluid dynamics in Equation 18. This one-way coupling allows the $Y_\mathcal{B}$ conservation equation to be independent of the other independent variables. Using the method of characteristics, the coupled system can be solved and the incoming wave eliminated.

Unfortunately, in the case of a single reversible reaction, the derivatives with respect to specific volume and pressure do not become zero far from the reaction zone. The $Y_\mathcal{B}$ conservation equation remains dependent on the other independent variables. In this case, we can define $\tau = \left(\frac{\partial \dot{\Omega}_\mathcal{B}}{\partial Y_\mathcal{B}}\right)^{-1}$, the *near equilibrium relaxation time*. This time scale represents the "relaxation time for small departures of $Y_\mathcal{B}$ from an equilibrium state at constant" v and P [13]. Using τ, we can re-express the $Y_\mathcal{B}$ conservation equation (Equation 4)

$$\frac{\mathrm{D}Y_\mathcal{B}}{\mathrm{D}t} = \frac{Y^{1*}_\mathcal{B} - Y^1_\mathcal{B}}{\tau} \tag{31}$$

In this expression, $Y^{1*}_\mathcal{B}$ is the difference between the bulk flow mass fraction ($Y^o_\mathcal{B}$) and $Y^*_\mathcal{B}$, the equilibrium value of $Y_\mathcal{B}$. With this new expression of the product species equation, we can also re-express the product net production rate ($\dot{\Omega}_\mathcal{B}$) derivatives and pseudo-thermodynamic function ($Z(v, P, \mathbf{Y})$) derivatives.

$$\dot{\Omega}_{Y_\mathcal{B},v} = -\frac{Y^*_{\mathcal{B},v}}{\tau} \quad \dot{\Omega}_{Y_\mathcal{B},P} = -\frac{Y^*_{\mathcal{B},P}}{\tau} \quad \dot{\Omega}_{Y_\mathcal{B},Y_\mathcal{B}} = \frac{1}{\tau} \tag{32}$$

$$Z_{,v} = a_f^2 \frac{h_{,Y_\mathcal{B}}}{h_{,\rho}} \frac{Y^*_{\mathcal{B},v}}{\tau} \quad Z_{,P} = a_f^2 \frac{h_{,Y_\mathcal{B}}}{h_{,\rho}} \frac{Y^*_{\mathcal{B},P}}{\tau} \quad Z_{,Y_\mathcal{B}} = -a_f^2 \frac{h_{,Y_\mathcal{B}}}{h_{,\rho}} \frac{1}{\tau} \tag{33}$$

To determine the characteristic wave speeds speeds necessary for the wave decomposition, we assume a Fourier form for the x-dependence of the perturbations (see Equation 17).

$$\mathbf{z}^1(x) = \mathbf{z}' \exp\left[-\frac{\omega}{\mathrm{c}} x\right] \tag{34}$$

We insert this functional form into Equation 29 and rearrange to determine the follow algebraic eigenvalue problem

$$\mathbf{A}_\infty^{-1}\left[\mathbf{I}+\frac{ik_y}{\omega}\mathbf{B}+\frac{1}{\omega}\mathbf{C}\right]_\infty \mathbf{z}' = \frac{1}{c}\mathbf{z}' \tag{35}$$

The eigenvalues of this equation (c) are exactly the characteristic wave speeds necessary for the wave decomposition. The characteristic polynomial associated with Equation 35 is

$$-\omega\tau^*\left(\frac{a_e}{a_f}\right)^2\left[c-\mathrm{u}_o\right]\left[\left(c-\mathrm{u}_o\right)^2-a_f^2\right]+c\left[\left(c-\mathrm{u}_o\right)^2-a_e^2\right]=0 \tag{36}$$

where a_f and a_e are the frozen and equilibrium soundspeeds, c is the characteristic wave speed, and τ^* is a function of τ [13]. Vincenti and Kruger [13] discuss the limits of this equation. As τ^* approaches zero, the time required for the composition to return to equilibrium becomes negligible and the second term in Equation 36 $\left(c\left[\left(c-\mathrm{u}_o\right)^2-a_e^2\right]\right)$ dominates. In this case, the characteristic wave speeds are: u, $\mathrm{u}+a_e$, $\mathrm{u}-a_e$. On the other hand, as τ^* approaches infinity, the time required for the composition to return to equilibrium becomes prohibitively long and the first term in Equation 36 $\left(\left[c-\mathrm{u}_o\right]\left[\left(c-\mathrm{u}_o\right)^2-a_f^2\right]\right)$ dominates. In this extreme, the characteristic wave speeds are: u, $\mathrm{u}+a_f$, $\mathrm{u}-a_f$.

In one-dimensional non-reactive fluid mechanics, there are three real characteristic wave speeds: u, $\mathrm{u}+a_f$, and $\mathrm{u}-a_f$. In one-dimensional systems with single step reversible chemical kinetics, there are four complex characteristic waves speeds given by Equation 36. For the limiting case of an irreversible reaction, there is a single soundspeed ($a_f = a_e$), and Equation 36 has an analytic solution. This solution is depicted in Figure 3 by the open squares. If the kinetics are reversible, there is not an analytic solution to Equation 36. Figure 3 shows numerically determined roots for varying extents of reversibility. The roots are labeled according to their non-reactive analogs. Only one root, the analog to $\mathrm{u}-a$, consistently has a negative real part and therefore corresponds to the incoming wave.

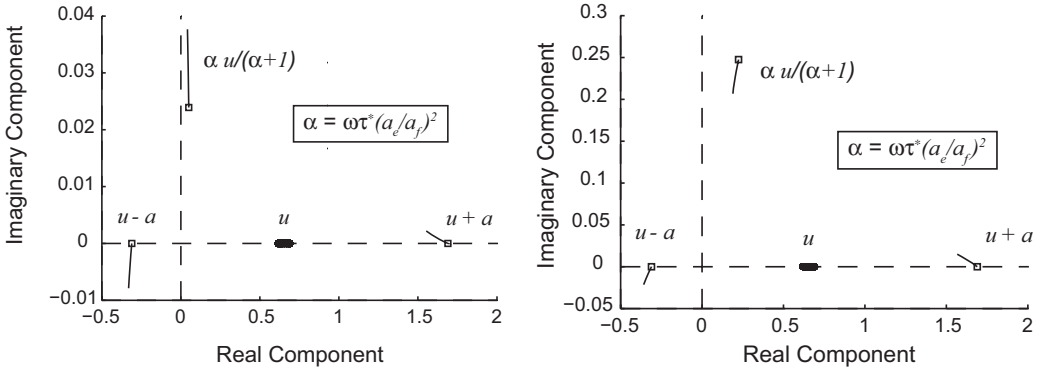

Figure 3: Roots (c) of Eq. 36 for the first two modes [2] normalized by the frozen soundspeed a_f. (a) Mode 1 (b) Mode 2

Once we have determined the characteristic wave speeds, i.e. the eigenvalues of Equation 35, we can find the corresponding right eigenvectors ($\mathbf{n}_i$) and express the perturbations far from the reaction zone as a superposition of waves.

$$\mathbf{z}' = \sum_{i=1}^{k} F_i \mathbf{n}_i \tag{37}$$

In this decomposition, F_i is a generic wave function which can be found by projecting the solution onto the left eigenvector $\mathbf{m}_i$

$$\mathbf{m}_i \cdot \mathbf{z}' = F_i(x - c_i t) \tag{38}$$

Finally, we insist that the wave function corresponding to the incoming wave be zero. Requiring that the incoming component of the solution be zero is equivalent to the requiring that the inner product of the solution vector and the left eigenvector $\mathbf{m}_i^*$ corresponding to the eigenvalue of Equation 36 with the negative real part be zero, i.e.

$$\mathbf{m}_i^* \cdot \mathbf{z}' = 0 \qquad (\mathcal{R}e(c_i^*) < 0) \tag{39}$$

In the case of an irreversible reaction, there is an analytic expression for this inner product.

$$\begin{aligned} Y'_{\mathcal{B}} &\left[(q(\gamma-1)) \left(\frac{-\dot{\Omega}_{Y_{\mathcal{B}},Y_{\mathcal{B}}} \mathrm{u}}{a_f^2} \right) \left(\frac{-\dot{\Omega}_{Y_{\mathcal{B}},Y_{\mathcal{B}}} \mathrm{u} \frac{\alpha}{\omega} + a_f \left(\omega - \dot{\Omega}_{Y_{\mathcal{B}},Y_{\mathcal{B}}} - \frac{(k_y \mathrm{u})^2}{\omega} \right)}{a_f^2 \left[(\omega - \dot{\Omega}_{Y_{\mathcal{B}},Y_{\mathcal{B}}})^2 - (k_y \mathrm{u}_\infty)^2 \right] - (\dot{\Omega}_{Y_{\mathcal{B}},Y_{\mathcal{B}}} \mathrm{u})^2} \right) \right]_\infty \\ &= \frac{\mathrm{u}'}{a_{f\infty}} - \frac{i k_y \mathrm{u}_\infty}{\omega} \frac{\mathrm{v}'}{a_{f\infty}} - \frac{\alpha_\infty}{\omega} \frac{P'}{\gamma P_\infty} \end{aligned} \tag{40}$$

The ∞ indicates that we evaluate the quantities far from the reaction zone where the system is almost in equilibrium. We recognize that in one dimension ($k_y = 0$), this reduces to Lee and Stewart's result, and in two dimensions neglecting chemical effects ($k_y \neq 0, Y'_{\mathcal{B}} = 0$), it reduces to Short's result. Because there is not an analytic solution for the reversible case, we use the LAPACK routine ZGEEV to numerically determine the eigenvalue and eigenvector of interest. The shooting method ensures that the radiation boundary condition is satisfied within a user-specified tolerance. We have used Muller's method [14] to satisfy our tolerance, but historically a two-dimensional Newton-Raphson method has been used [2]. In a large multi-step mechanism with reversible reactions, we believe that this method will be applicable.

3 Results

Using the methodology outlined above and the family of single step reactions with constant T_{CJ}, we have investigated the unstable modes for nine extents of reversibility

$$\Delta s/R = 0, -1, -2, -3, -4, -5, -6, -7, -8 \tag{41}$$

The ZND profiles normalized by the post-shock state of the two extreme cases ($\Delta s/R = 0$ and $\Delta s/R = -8$) are depicted in Figure 4. As given in Table 1, $\Delta s/R = 0$ corresponds to an irreversible reaction where the reactant is completely consumed at equilibrium. $\Delta s/R = -8$ corresponds to a case where approximately half of the reactant is consumed at equilibrium. The most visible difference in the ZND profiles is the change in the energy pulse width ($\Delta_{e,ZND}$) [15]. As the reaction becomes more reversible, the energy release zone becomes more concentrated. Figure 5 shows eigenfunctions for the two extreme cases ($\Delta s/R = 0$ and $\Delta s/R = -8$) at the lowest overdrive value ($f = 1.2$). The complex growth rates for these eigenfunctions are $\omega = 0.657 + i0.320$ and $\omega = 0.526 + i0.558$ respectively. As in the ZND profiles shown in Figure 4, we see that the energy release zone is more concentrated in the more reversible system. Otherwise, the profiles are relatively similar.

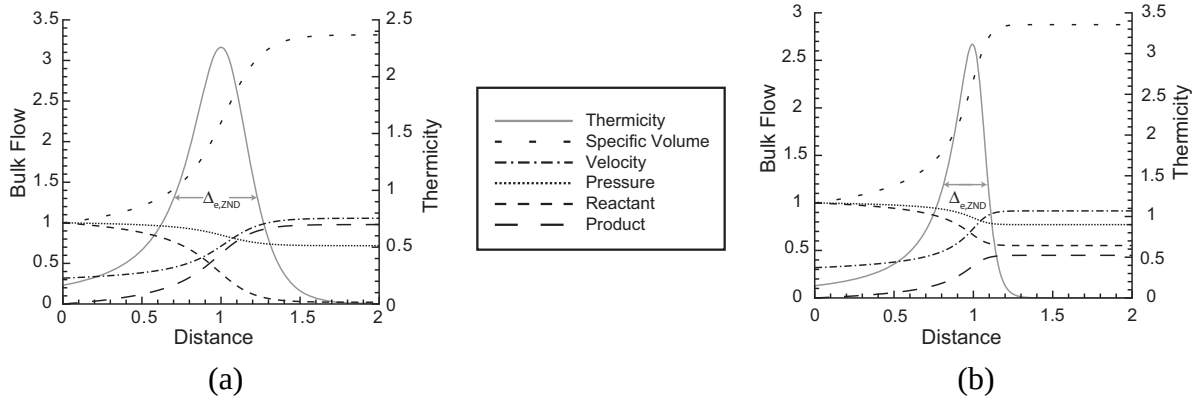

Figure 4: ZND structure for two extents of reversibility (a) $\Delta s/R = 0$ (b) $\Delta s/R = -8$ normalized by the post-shock state.

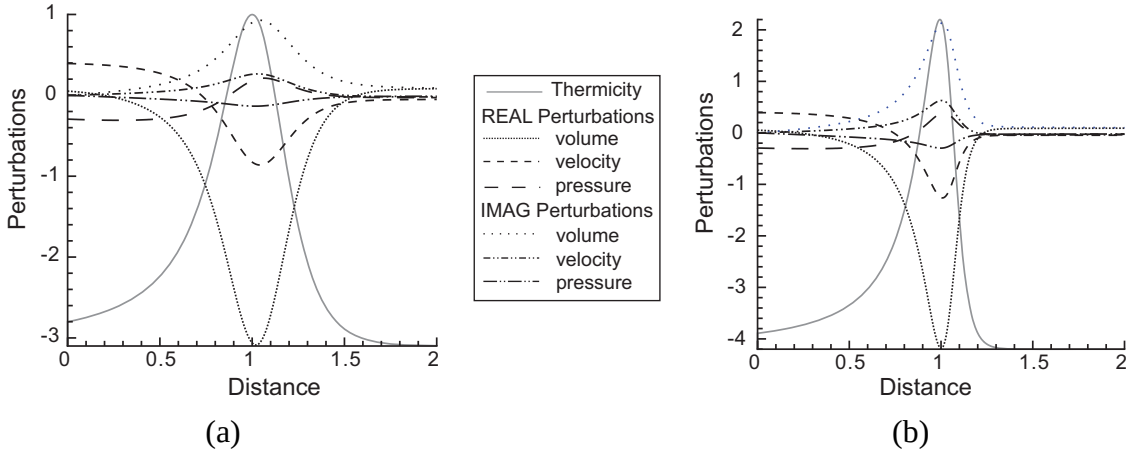

Figure 5: Eigenfunction profiles ($\mathbf{z}^1(x)$) for the lowest mode, $f = 1.2$, and two extents of reversibility (a) $\Delta s/R = 0$ (b) $\Delta s/R = -8$

Figure 8 shows the values of the complex growth rate (ω) with positive growth rates for varying values of overdrive (f). The first four modes of instability are shown, and the black squares indicate

the results for the irreversible one step reaction model from Lee and Stewart's paper [2]. These data points agree with our $\Delta s/R = 0$ curve which is expected. Additionally, as the mode number increases, the number of unstable growth rates decreases for a given extent of reversibility which again agrees with Lee and Stewart's results. Figures 5a, 6a, and 6b show modes one, two, and three respectively for $\Delta s/R = 0$ for $f = 1.2$ illustrating how the eigenfunctions change with mode.

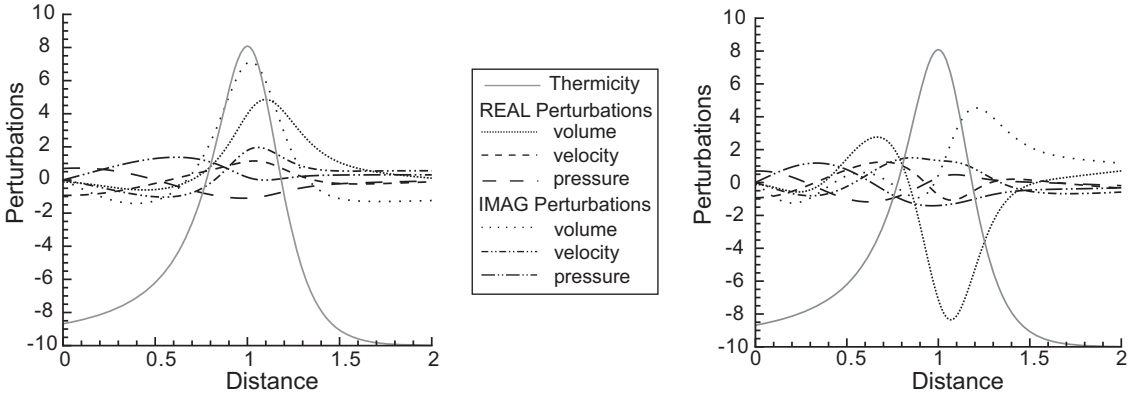

Figure 6: Eigenfunction profiles ($\mathbf{z}^1(x)$) for $\Delta s/R = 0$, $f = 1.2$, and two modes (a) Mode 2 (b) Mode 3

Table 2 and Figure 7 illustrate the neutral stability curves ($\mathcal{R}e(\omega) = 0$) for modes one through four. For mode one, increasing reversibility has a stabilizing effect so that as the system becomes more reversible, the overdrive corresponding to the neutral stability decreases. On the other hand, for modes two, three, and four, reversibility has a destabilizing effect. Alpert and Toong [16] give a discussion of the mechanism of the longitudinal oscillation in a square-wave detonation. They observed two distinct frequencies of oscillation in hydrogen and oxygen, a low frequency mode ($3.8 - 5.4\Delta_{i,ZND}$) and a high frequency mode ($\approx 1.6\Delta_{i,ZND}$). Although we have not performed direct Euler simulations to observe the wave structure of our reversible reaction model, mode one may behave differently than modes two, three, and four because it represents the low frequency mode while modes two through four represent the high frequency mode.

Table 3 gives the value of the near equilibrium relaxation times (τ) for each extent of reversibility, τ^* from Equation 36, the energy release pulse width times ($\tau_{e,ZND}$) determined from the base flow thermicity profile, and the inverse of the frequencies for the lowest overdrive value ($f = 1.2$) at each mode level. As the mode number increases, the imaginary part of the complex growth rate ($\mathcal{I}m(\omega)$) also increases. The values in Table 3 indicate that for mode one, the period of perturbation oscillation ($1/\mathcal{I}m(\omega)$) is two orders of magnitude greater than the chemical equilibration time scale (τ). As the mode number increases and the frequency increases, the period of the perturbation oscillation decreases, but still remains approximately a factor of two greater than the chemical equilibration scale. This indicates that we are still in the equilibrium regime of Equation 36 and the period of the perturbation is long enough that it allows the composition to remain in equilibrium. On the other hand, ($1/\mathcal{I}m(\omega)$) is an order of magnitude larger than $\tau_{e,ZND}$ for mode one, comparable for mode two, approximately half for mode three, and an order of magnitude less for mode four. This may indicate that higher modes are excited more when their period becomes comparable to or less than the energy release pulse width.

$\Delta s/R$	$f_{\mathcal{R}m(\omega)=0}$			
	Mode 1	Mode 2	Mode 3	Mode 4
0	1.723	1.577	1.398	1.290
-2	1.694	1.592	1.423	1.317
-4	1.653	1.617	1.469	1.370
-6	1.629	1.645	1.516	1.426
-8	1.617	1.671	1.558	

Table 2: Neutral stability ($\mathcal{R}e(\omega) = 0$) overdrive values for modes one through four with varying extents of reversibility.

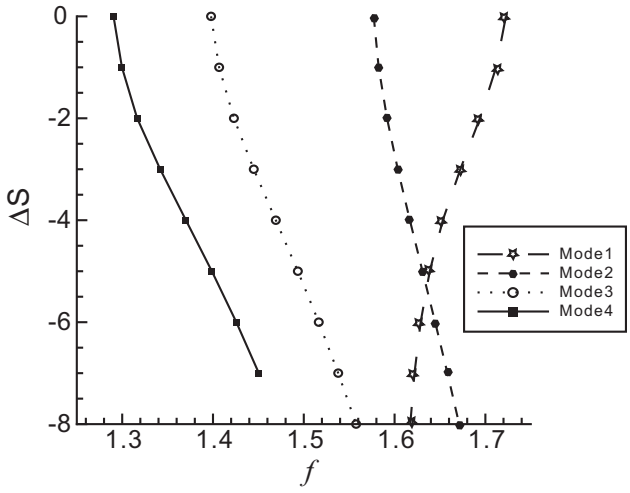

Figure 7: Neutral stability ($\mathcal{R}e(\omega) = 0$) curves for modes one through four with varying extents of reversibility.

4 Conclusions

We have implemented the normal modes approach [2] to linear stability of detonations for an ideal gas with an arbitrary kinetics mechanism. When reversible reactions are included, no analytic solution for the radiation condition exists because the one-way coupling between fluid mechanics and chemistry no longer exists far from the reaction zone, and unlike, non-reactive systems, the characteristic speeds in reactive systems are complex. We have proposed a generalized wave decomposition method that we believe is applicable for all gaseous systems. Our new method constructs and algebraic eigenvalue problem far from the reaction zone (Equation 35). We find the complex eigenvalues of this problem which correspond to the the characteristic wave speeds and determine the eigenvector that corresponds to the eigenvalue with a negative real component. Finally, we require that the inner product of this eigenvector and the solution vector be zero (Equation 39).

Using this new model, we have studied the stability characteristics of a system consisting of a single reversible reaction between two perfect gases. Our results indicate that reversibility has a stabilizing effect on the lowest mode and a destabilizing effect on higher modes. The near

$\Delta s/R$	τ (s)	τ^* (s)	$\tau_{e,ZND}$	$1/\mathcal{I}m(\omega)$ (s)			
				Mode 1	Mode 2	Mode 3	Mode 4
0	0.0498	0.0474	0.286	3.125	0.220	0.121	0.0844
-2	0.0520	0.0409	0.269	2.57	0.218	0.121	0.0841
-4	0.0563	0.0309	0.232	2.10	0.216	0.120	0.0834
-6	0.0601	0.0231	0.193	1.89	0.214	0.119	0.0826
-8	0.0627	0.0179	0.163	1.79	0.213	0.118	

Table 3: Near equilibrium relaxation time (τ) and τ^* (Eqn 36) for varying extents of reversibility. Complex growth rates for modes one and four are given for the lowest overdrive value ($f = 1.2$).

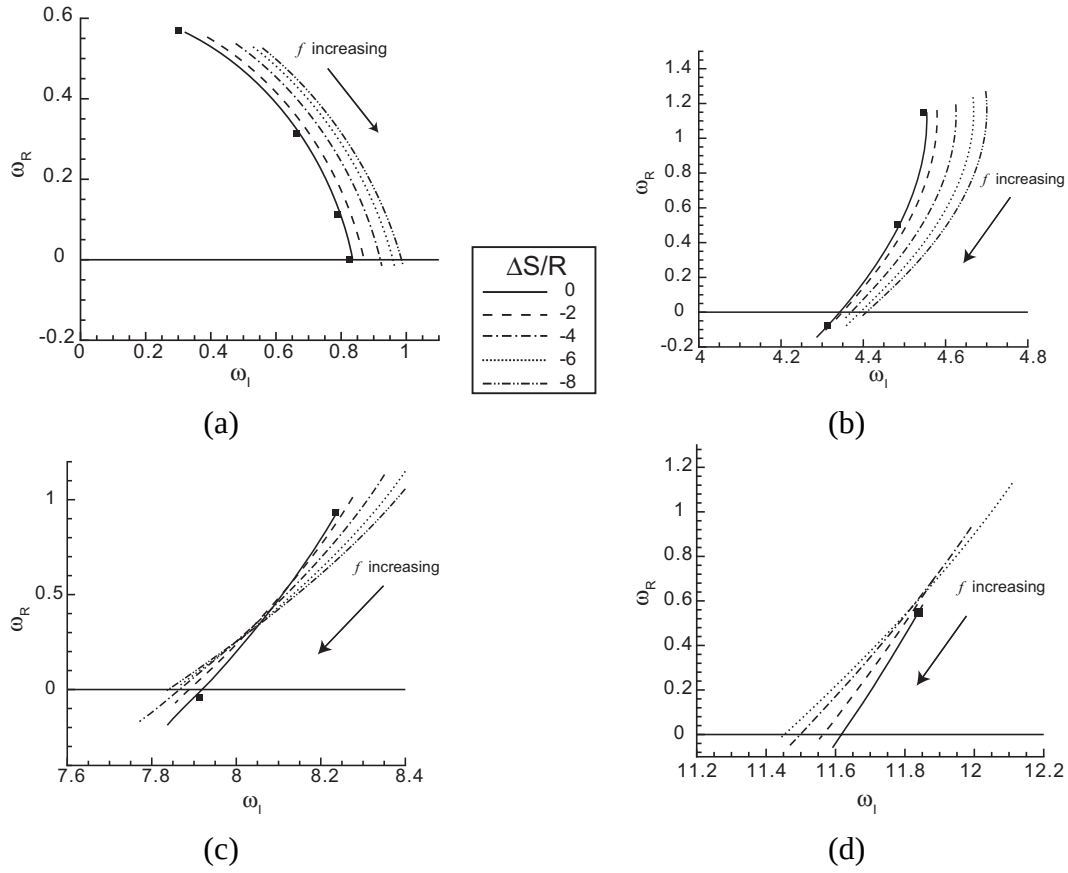

Figure 8: Unstable roots for the first four modes. (a) Mode 1 (b) Mode 2 (c) Mode 3 (d) Mode 4

equilibrium relaxation time (τ) indicates that for the parameter space we have studied, the system remains in equilibrium, but that the relationship between the period of oscillation ($1/\mathcal{I}m(\omega)$) and the energy pulse release width ($\tau_{e,ZND}$) varies with the mode number.

In the future, we plan to perform direct Euler simulations to validate our complex growth rates. The results of direct Euler simulations will also provide wave structures that can be compared with Alpert and Toong's results [16]. Then, we plan to investigate the effect of reversibility on two dimensional perturbations ($k_y \neq 0$). Eventually, we hope to use our formulation with detailed

kinetics mechanisms to determine unstable modes for realistic chemical systems.

5 Acknowledgments

This work was supported by the ASC Center for Simulation of Dynamic Response of Materials is based at the California Institute of Technology under U. S. Department of Energy contract W-7405-ENG-48.

References

[1] D. S. Stewart and A. R. Kasimov. *J. Propulsion Power*, 22 (2006) 1230–1244.

[2] H. I. Lee and D. S. Stewart. *J. Fluid Mech.*, 216 (1990) 103–132.

[3] M. Short. *SIAM J. Appl. Math.*, 57 (1997) 307–326.

[4] M. Short and D. S. Stewart. *J. Fluid Mech.*, 368 (1998) 229–262.

[5] M. Short and J. J. Quirk. *J. Fluid Mech.*, 339 (1997) 89–119.

[6] Z. Liang and L. Bauwens. *Combust. Theor. Model.*, 9 (2005) 93–112.

[7] J. J. Erpenbeck. *Phys. Fluids*, 5 (1962) 604–614.

[8] Ia. B. Zel'dovich. *Zh. Eksp. Teor. Fiz.*, 10 (1940) 542–568.

[9] J. von Neumann. Theory of detonation waves. In A. J. Taub, editor, *John von Neumann, Collected Works*. Macmillan, New York, 1942.

[10] W. Doering. *Ann. Phys.*, 43 (1943) 421–436.

[11] S. D. Cohen and A. C. Hindmarsh. *Computers in Physics*, 10 (1996) 138–143.

[12] D. Goodwin. Cantera: Object-oriented software for reacting flows. Technical report, California Institute of Technology, 2005.

[13] W. G. Vincenti and C. H. Kruger. *Introduction to Physical Gas Dynamics*. Krieger Publishing Company, 1965.

[14] J. Stoer and R. Bulirsch. *Introduction to Numerical Analysis*. Springer-Verlag, 1983.

[15] Z. Liang, S. Browne, R. Deiterding, and J. E. Shepherd. Detonation front structure and the competition for radicals. In *Proc. Combust. Inst.*, Vol. 31, 2007.

[16] R. L. Alpert and T. Y. Toong. *Astronautica Acta*, 17 (1972) 539–560.